J Solid State Electrochem (2010) 14:63–70
DOI 10.1007/s10008-009-0785-6

ORIGINAL PAPER

Seed layer-free electrodeposition and characterization of vertically aligned ZnO nanorod array film

Feng Xu · Yinong Lu · Yan Xie · Yunfei Liu

Received: 5 October 2008 / Revised: 2 December 2008 / Accepted: 3 January 2009 / Published online: 27 January 2009

Abstract Vertically aligned arrays of ZnO nanorod (ZNR) were rapidly synthesized on ITO glass without needing a pre-prepared seed layer of ZnO via a hexamethylenetetramine (HMT)-assisted electrodeposition route. The effect of HMT on the ZNR electrodeposition process was investigated by the cyclic voltammetric curve and the current–time curve. An electrodeposition growth model based on the capping effect of HMT–4H was proposed. The as-synthesized ZNRs possess single crystalline, a wurtzite crystal structure with markedly preferential growth orientation along [0001] direction determined by transmission electron microscopy and powder X-ray diffraction. As compared with the electrodeposited ZnO film without HMT assistance, the ZNR arrays showed the high transmittance (90%) in the visible wavelength range and the blue-shift of the band gap energy. Moreover, the presence of an optical-phonon E_2 (high) at 437.3 cm^{-1} in Raman spectrum and strong ultraviolet emission at 376 nm but weak defect-related deep level emission in the room temperature photoluminescence spectrum also indicated that such ZNR arrays are of good crystal quality. More importantly, the rapid synthesis of ZNRs could provide the feasibility for preparation of ZnO nanotubes within a shorter time by a subsequent electrochemical dissolution process.

Keywords Zinc oxide · Electrodeposition · Nanowire arrays · Optical properties · Nanotube arrays

F. Xu · Y. Lu (✉) · Y. Xie · Y. Liu
State Key Laboratory of Materials-Oriented Chemical Engineering, College of Materials Science and Engineering, Nanjing University of Technology,
Nanjing 210009, China
e-mail: ynlu@njut.edu.cn

Introduction

One-dimensional (1D) semiconductor nanostructures such as rods [1, 2], wires [3], belts [4], and tubes [5, 6] have attracted much attention due to their unique optical and electronic properties that are useful in future electronic and photonic devices. Among many oxide semiconductors, ZnO, a wide direct band gap (E_g=3.37 eV) semiconductor with large exciton binding energy (60 meV) at room temperature [7], has been extensively investigated because of its great potential use in piezoelectric transducers [8], optical waveguides [9], surface acoustic wave filters [10], chemical and gas sensors [11], light-emitting diodes [12], and dye-sensitized solar cells [13]. Various vapor-phase methods such as the vapor–liquid–solid epitaxial [14], pulsed laser deposition [15], and metal-organic chemical vapor deposition [16] have been successfully used to grow oriented ZnO nanorod (ZNR) and nanowire (ZNW) arrays at relatively high temperature of 800–900 °C. Besides the limitations of a high preparation temperature and energy-consuming experiment facilities, these vapor-phase methods usually need costly and/or insulting substrates, such as sapphire, titanium nitride, or gallium nitride, for epitaxial growth. Recently, a hydrothermal approach to the growth of vertically aligned ZNR and ZNW arrays was developed by Vayssieres [17]. They utilized the seed-layer-induced hydrothermal method to prepare 1D ZNR arrays on silicon or glass substrates, which were performed under high pressure in an autoclave. However, the typical growth rate in the hydrothermal process is relatively low. Furthermore, the interface quality in the presence of seed layer is not ideal due to the existing defects leading to low adhesion, low thermal, and electrical transport.

In order to overcome these limitations, the cathodic electrodeposition of ZnO films has triggered considerable interests due to its distinctive advantages such as the precise

control over the film thickness and morphology, the possibility to prepare films with large area, relatively high deposition rate, low growth temperature, and low cost. The most important aspect in the electrochemical deposition of ZnO is the reduction of an oxygen precursor at the interface of electrode and precursor solution, which controls the growth rate and affects the crystallinity and morphology of obtained film significantly. Three kinds of oxygen precursor have been reported up to now, i.e., nitrate ions (NO_3^-), dissolved molecular oxygen (O_2), and hydrogen peroxide (H_2O_2). In 1996, Peulon et al. prepared ZnO films of good quality for the first time by direct electrodeposition from aqueous solution containing dissolved molecular oxygen [18]. Lately, Tena-Zaera et al. investigated the role of chloride ions on electrodeposition of ZnO nanowire arrays from O_2 reduction on the substrate with ZnO seed layer [19]. Compared with the dissolved molecular oxygen precursor, the zinc nitrate ($Zn(NO_3)_2$) solution can act as both the zinc and oxygen precursor, which will widen the adjustable range of oxygen concentration. However, only hexagonal ZnO particles [20] or pillars [21] were electrodeposited from the single $Zn(NO_3)_2$ electrolyte.

Herein, we used a hexamethylenetetramine (HMT)-assisted electrodeposition route to obtain large-sacle, dense ZNR arrays on smooth ITO substrates without needing a pre-prepared ZnO seed layer within a short time. Although HMT has newly been used in the electrodeposition of aligned arrays of ZNRs [22] and ZNWs [23], one important issue still remains as to how HMT favor wire or rod growth rather than dense hexagonal ZnO particle growth during the electrodeposition process. In this paper, the effect of HMT on the ZNR electrodeposition process in the $Zn(NO_3)_2$ aqueous solution was studied by the cyclic voltammetric (CV) curves and the current–time curves. A new electrodeposition growth model for ZNRs was tentatively proposed for the first time. The structure, morphology, and chemical composition of the samples were characterized, and the optical properties of obtained ZNR arrays were investigated. Electrodeposited ZnO films or ZNR arrays have shown tunability in the optical band gap depending on the structural morphology obtained. In addition, as-electrodeposited ZNR arrays show strong UV emissions at room temperature as well as weak defect-related deep level emission (DLE) in the visible region. More importantly, on the basis of rapid synthesis of ZNRs, the formation of arrays of ZnO nanotube (ZNT) can also be achieved by a subsequent electrochemical dissolution process within a total time of 30 min.

Experimental

All chemicals purchased from Shanghai Chemical Reagents Co. Ltd. were of analytical reagent grade and used as received without further purification. In a typical procedure, the ZNR arrays on ITO substrates were electrodeposited from an equimolar (0.01 M) hybrid aqueous solution of $Zn(NO_3)_2$ and HMT with initial solution pH of 5.5±0.1. Prior to each experimental run, the ITO substrate with a sheet resistance of about 10–15 Ω/□ was thoroughly cleaned using detergent without further treatment. The electrodeposition was potentiostatically performed on a ZF–3 potentiostat (Shanghai Zhengfang Electron Co., China), using a classical three-electrode configuration, in which an ITO substrate, a graphite rod and a saturated calomel electrode (SCE) served as the working electrode (cathode), the counter electrode, and the reference electrode, respectively. Bath temperature was kept at a constant temperature of 70 °C. A SCE was immersed in saturated KCl solution that was connected to the electrolyte bath with a Luggin capillary. The space width between the working electrode and the counter electrode is about 5 cm, and the effective area of the working electrode is 2 cm^2. The applied potential and the duration of the depositions were –1.0 V versus SCE and 5–60 min, respectively. At the end of each growth period, the ITO substrate covered with ZNRs was removed from the solution and immediately rinsed in flowing deionized water to eliminate any residual impurities from the surface.

The secondary electron images (SEIs) from a scanning electron microscope (JSM-5900, JEOL Ltd., Japan) were employed for the observation of the surface morphology of the electrodeposited samples. Chemical compositions of the as-prepared samples were obtained using an energy-dispersive spectrometer (EDS, Noran Vantage DSI, Themo Noran, Middleton, WI, USA). Their crystallographic characterization was investigated by an X-ray diffractometer (XRD; ARL XTRA, Themo Electron Co., USA) with Cu $K\alpha_B$ radiation. Transmission electron microscopic (TEM) images were performed with a high-resolution TEM (HRTEM; JEM-2010, JEOL Ltd., Tokyo, Japan) operated at 200 kV. Optical transmittance of the ZNR arrays was carried out by a Shimadzu UV-3101PC UV-vis-near infrared spectrophotometer. A blank ITO glass was used as a reference to eliminate the interference of the substrate. Raman scattering experiment was performed using a microscopic confocal Raman spectrometer (JY HR 800, Jobin Yvon Ltd., France) with a 514.5-nm Ar^+ laser operated at 2 mW. The spectrum was recorded in backscattering configurations when the incident light was normal to the sample surface. The photoluminescence spectra were measured at room temperature with a spectrophotometer (Jobin Yvon Fluorolog3-221) using a Xe lamp (450 W) as excitation source.

Results and discussion

Figure 1a–d display the typical plan-view and cross-sectional SEIs of electrodeposited ZnO films from 0.01 M

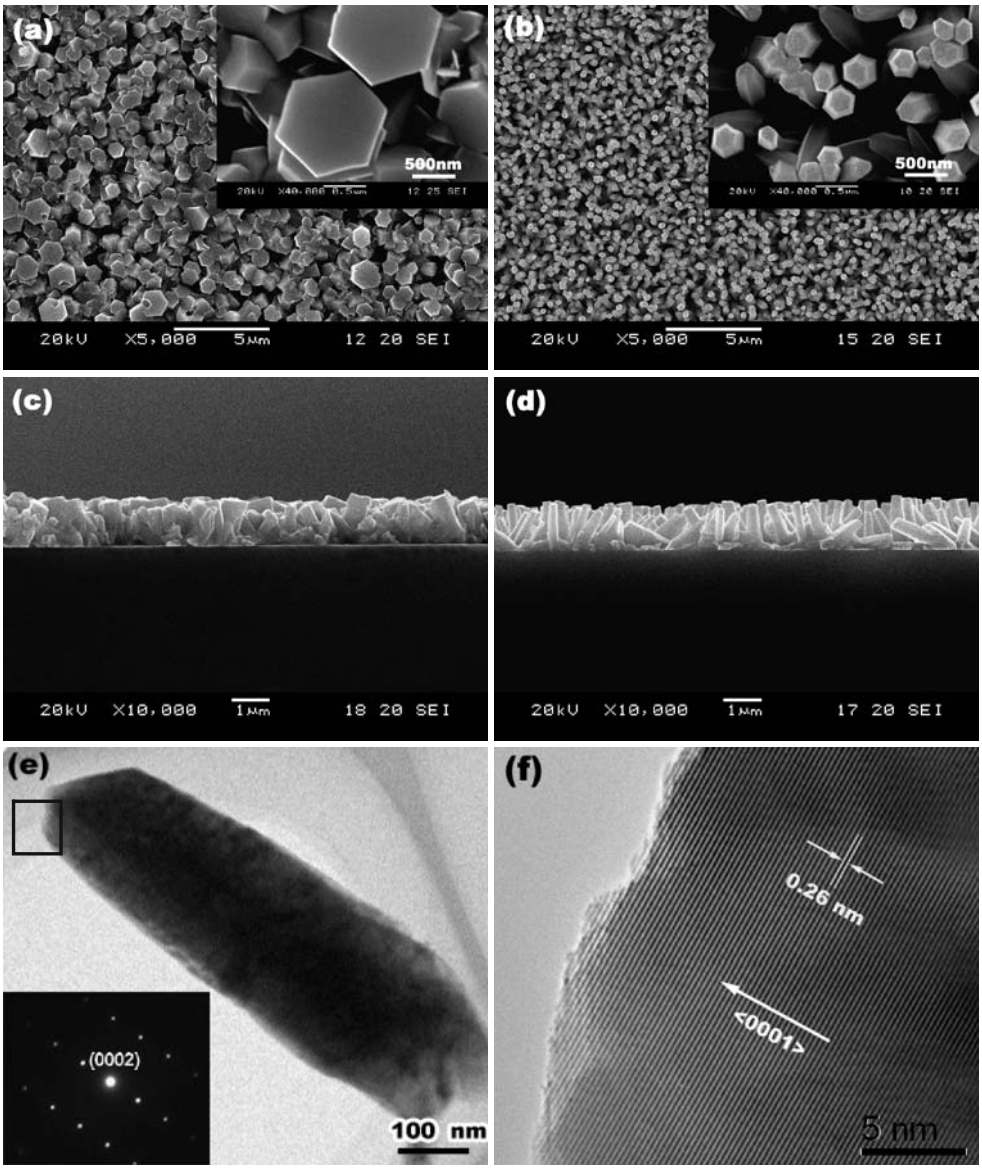

Fig. 1 Plan-view SEIs of the ZnO films electrodeposited in Zn $(NO_3)_2$ aqueous solution **a** without and **b** with HMT at 70 °C and –1.0 V for 20 min; **c** and **d** correspond to cross-sectional SEIs of **a** and **b**, respectively. The *insets* in the upper right corner in **a** and **b** show enlarged view of the corresponding images. **e** Low-resolution TEM image of an individual ZNR peeled from the ITO glass substrate and its corresponding SAED pattern (*inserted* at the bottom left corner). **f** HRTEM image taken from the area marked with the black frame in **e**

$Zn(NO_3)_2$ aqueous solution without and with HMT at 70°C and –1.0 V when the deposition duration is 20 min. The insets in upper right in Fig. 1a and b show the enlarged views of the corresponding images. It can be seen from Fig. 1a that ZnO film deposited from HMT-free $Zn(NO_3)_2$ aqueous solution is composed of regular well-defined single-crystalline hexagonal columns with diameters of 0.5–1.2 μm. With the introduction of HMT to the electrolyte, the surface morphology of the film changed dramatically. Figure 1b shows a large area of vertically aligned ZNR arrays grown on ITO glass substrate. The ZNRs are very highly oriented and vertically formed on the entire ITO substrate with diameter of about 200–300 nm. The cross-sectional SEIs corresponding to Fig. 1a displays that the film consists of agglomerated ZnO columns, as shown in Fig. 1c. Whereas, the cross-sectional SEIs corresponding to Fig. 1b shows that ZNR array film is composed of numerous separate ZNRs (Fig. 1d) with their *c*-axes perpendicular to the substrate. It can also be seen from the cross-sectional morphologies that both the films deposited without and with HMT are strongly adherent to the substrate, with thickness of approximately 1.3 μm. It is calculated that the growth rate for ZNR array film is about 65 nm/min, which is much faster than parallel in the hydrothermal process [17].

Further structural characterizations of the ZNRs were performed by TEM and HRTEM. To prepare TEM samples, the ZNRs were scraped from the ITO glass substrate onto a holey amorphous carbon-film-covered copper grid. Figure 1e shows the low-resolution TEM image of an individual ZNR with a diameter of approximately 200 nm. The corresponding SAED pattern of the ZNR (inserted at the bottom left corner of Fig. 1e) can be indexed to wurtzite structure of hexagonal ZnO and indicates its single-crystal

nature and its growth direction along [0001]. The typical HRTEM image, taken from the area marked with the black frame in Fig. 1e, is illustrated in Fig. 1f. The crystal lattice fringes are clearly detected and average distance between the adjacent lattice planes is 0.26 nm that also corresponds well to the interplanar distance of the (0001) crystal planes of wurtzite ZnO, which further proves that ZNRs prepared in the present system grow along *c*-axis.

The XRD patterns of as-electrodeposited ZnO column film and ZNR array film are presented in Fig. 2. Both the XRD patterns can be indexed as wurtzite (hexagonal) structured ZnO (space group $P6_3mc$) with cell parameters a=3.249 Å and c=5.206 Å, which is in good agreement with the literature values (JCPDS card, no. 36-1451). From these XRD data, we can illustrate the texture effect of the anisotropic morphology and orientation on the relative intensity of the diffraction peak (normalized to the $(10\bar{1}1)$), which usually corresponds to the maximum intensity of ZnO). As expected, a substantially higher intensity is observed for the (0002) diffraction peak in the XRD patterns of the ZNR arrays (Fig. 2b), indicating that the ZNRs are highly oriented with their *c*-axes being perpendicular to the ITO glass substrate, which is well consistent with the SEI result in Fig. 1d. For the XRD pattern of the ZNR arrays, both the extremely high intensity ratios of $I_{(0002)}/I_{(10\bar{1}1)}$ and $I_{(0002)}/I_{(10\bar{1}1)}$ suggest that the ZNR arrays exhibit a single-crystal-like structure [24]. Figure 3 shows the representative EDS result of the ZNRs prepared by an HMT-assisted aqueous electrodeposition. The EDS pattern indicates that the ZNRs are only composed of only Zn and O. Quantitative analysis shows that mean atomic ratio of Zn/O of the ZNRs is 0.465:0.535. No evidence of other impurities was detected, and the ZNRs are nearly stoichiometric. These data also confirm the high purity of the ZNRs.

Electrochemical reactions relevant to the film growth have been studied by the CV. Cyclic voltammograms recorded from aqueous solution of 0.01 M $Zn(NO_3)_2$ without and with HMT are shown in Fig. 4. The sweep is

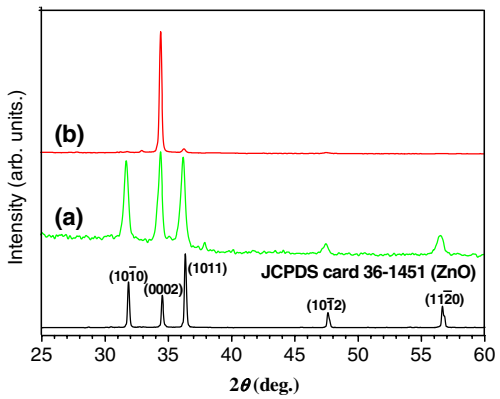

Fig. 2 XRD pattern of the as-electrodeposited ZnO column-like film (**a**) and ZNR array film (**b**)

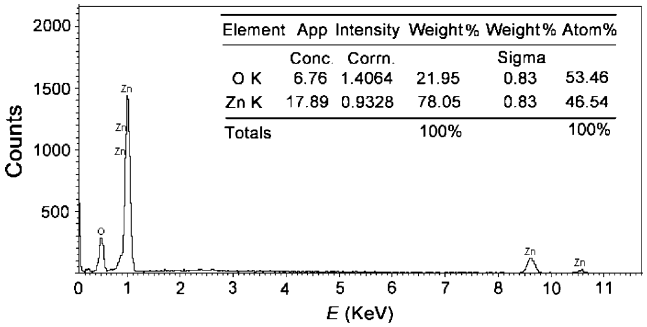

Fig. 3 Representative EDS result of the ZNRs prepared by a HMT-assisted aqueous electrodeposition

measured at a scan rate of 5 mV·s^{-1} over the potential range from 0 to –1.5 V. For the pure $Zn(NO_3)_2$ solution without HMT (Fig. 4a), virtually no current appears until the potential becomes more negative than about –0.6 V. Between –0.6 and –1.0 V, the cathodic current increases gradually with the potential. From –1.0 V, a steep increase of the cathodic current density takes place up to –1.9 mA/cm^2, which could be mainly ascribed to the deposition of metallic zinc ($E^{\circ}_{Zn^{2+}/Zn} = -1.07$ V vs. SCE at 25 °C) or the hydrogen evolution reaction [25]. The latter has been confirmed because a mass of bubbles generating from the ITO substrate surface were observed during the CV experiment. Commonly, in the case of $Zn(NO_3)_2$ solution system, only a small quantity of metallic zinc is deposited; thus, no reversible anodic peak corresponding to the striping of metallic zinc is detected [26], which is not in accordance with the instance of $ZnCl_2$ solution system [27]. The absence of anodic peak in the reverse scan also indicates the high stability of the formed ZnO. A plateau is observed between –0.8 and –1.0 V where the ZnO deposition is expected. The mechanism of deposition of ZnO film from $Zn(NO_3)_2$ aqueous solution has been developed as follows (Eqs. 1–4). First, cathodic reduction of nitrate ions liberates hydroxide ions in the vicinity of the

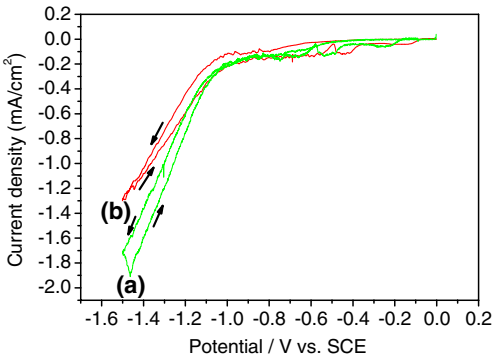

Fig. 4 Cyclic voltammograms measured at an ITO glass electrode in aqueous solutions of 0.01 M $Zn(NO_3)_2$ **a** without HMT and **b** with HMT at bath temperature of 70 °C. The sweep is measured at a scan rate of 5 mV s^{-1} over the potential range from 0 to –1.5 V

cathode (Eq. 1). Then, zinc ions deposit with hydroxyl anions (Eq. 2). Subsequently, zinc hydroxide spontaneously dehydrates into ZnO (Eq. 3) when the solution temperature is higher than 34 °C [28] and ultimately turns into ZnO film. An entire reaction is generally expressed as Eq. 4. Similar CV curve (Fig. 4b) is obtained when HMT is added to the $Zn(NO_3)_2$ aqueous solution. However, it can be found from Fig. 4 that for the $Zn(NO_3)_2$ solution with HMT, the corresponding cathodic current at the same potential is obviously lower than that of the HMT-free solution, indicating that the addition of HMT suppresses the electrochemical reaction to some extent.

$$NO_3^- + H_2O + 2e^- \rightarrow NO_2^- + 2OH^- \quad (1)$$

$$Zn^{2+} + 2OH^- \rightarrow Zn(OH)_2 \quad (2)$$

$$Zn(OH)_2 \rightarrow ZnO + H_2O \quad (3)$$

$$Zn^{2+} + NO_3^- + 2e^- \rightarrow ZnO + NO_2^- \quad (4)$$

Figure 5 presents the typical variation curve of the cathodic current density as the function of the time at 70 °C under constant deposition potential of –1.0 V for electrodeposition from 0.01 M $Zn(NO_3)_2$ solution without and with HMT. The time evolution plots of the observed current density enable us to track the film growth rate and especially to examine the effect of adding HMT. In the absence of HMT, the cathodic current density decreases sharply during the first 80 s and then abruptly increases to a stationary value of –0.39 mA/cm^2 in the following 220 s. When the deposition duration is from 20 to 50 min, the current density remains a rising tendency. When HMT is added, an analogous change in the current density is observed in the initial electrodeposition stage (Fig. 5b). As compared with Fig. 5a, b exhibits smaller fluctuation in the initial stage and then levels off in the subsequent electrodeposition. The steady current density for ZnO growth with HMT is slightly lower than that of the free-HMT solution, which agrees with the results from CV curves in Fig. 4.

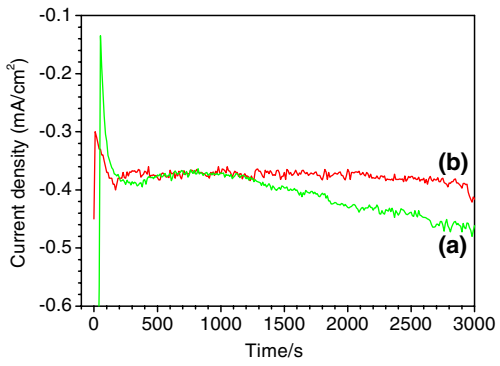

Fig. 5 Current density–time curves for electrodeposition at –1.0 V vs. SCE from aqueous solution of 0.01 M $Zn(NO_3)_2$ **a** without HMT and **b** with HMT at bath temperature of 70 °C

It is generally thought that HMT, as the nucleation-control reagent, is expected to release hydroxyl ions and acted as the organic template at elevated temperature in aqueous solution synthesis, thus dynamically modifying the nucleation process. Herein, while the solution was heated, HMT began to hydrolyze into OH^- and organic molecules $(CH_2)_6N_4$–4H (abbreviated as HMT–H4) according to Eq. 5 [29]. Thereby, before electrodeposition, $Zn(OH)_4^{2-}$ ions, the growing units have existed and adsorbed on the ITO surface. Any adsorption phenomenon at interface decreases the interfacial tension γ. Such effect is described quantitatively by Gibbs adsorption equation: $d\gamma = -\sum_i \Gamma_i d\mu_i$ [30], where Γ represents the superficial adsorption density and μ is the chemical potential of adsorbed species i. Reducing the interfacial tension leads to a great lowering of the nucleation energy barrier and more ZnO nucleus could adsorb on the substrate, which provides the likelihood for dense growth of the ZNRs. After commencement of electrodeposition, the negative nature of the growth unit $Zn(OH)_4^{2-}$ will lead to the different growth rates of planes, that is, $V_{(0001)} > V_{(10\bar{1}0)} > V_{(10\bar{1}\bar{1})} > V_{(10\bar{1}1)} > V_{(000\bar{1})}$. However, the generated HMT–H4 that bears four positive charges will preferentially adsorb on the negative polar planes (i.e., $(10\bar{1}0)$, $(10\bar{1}\bar{1})$, and $(10\bar{1}1)$ planes) by the coulomb interaction, retarding the lateral growth rate of these planes and enhancing the preferential growth of (0002) plane, as shown in Fig. 6. Besides, the presence of a mass of hydroxyl ions from HMT hydrolysis kinetically suppresses Eq. 1; thus, the current density for ZnO growth with HMT is slightly lower than that of the free-HMT solution, which is reflected in Figs. 4 and 5. Another possible explanation for the decrease in current density may be that the adsorption of HMT–H4 on the active sites of the electrode surface may block the adsorption of Zn^{2+} on these active sites, depressing the catalytic role of Zn^{2+} to reduction of nitrate [31]. The cathodic current is enhanced upon increasing the concentration of the adsorbed Zn^{2+} ions onto the electrode. Electrochemically, the electrodeposition conditions used in this paper resulted in a relatively fast electrochemical reduction of NO_3^- in comparison to the diffusion of Zn^{2+} to the cathode (ITO substrate). Consequently, ZnO was formed only at the tips of the vertical cylindrical crystals, quenching their lateral growth. Ultimately, the ZNRs are formed on the ITO substrate. A new electrodeposition growth model baded on the capping effect

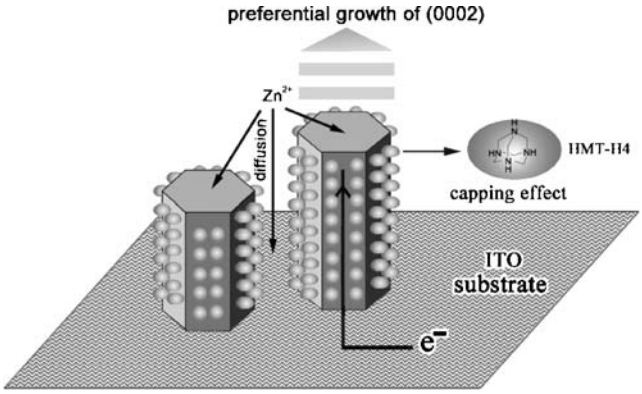

Fig. 6 The electrochemical growth model via an HMT-assisted electrodeposition route

of HMT−4H and the restricted diffusion of Zn^{2+} ions was proposed, as illustrated in Fig. 6.

$$(CH_2)_6N_4 + 4H_2O \rightarrow (CH_2)_6N_4 - 4H + 4OH^- \quad (5)$$

Figure 7 shows the optical transmittance spectra of the ZNR arrays as well as that of the ZnO column-like film. The inset in Fig. 7 shows the plot of $(-\ln(T)\cdot h\nu)^2$ versus photon energy of the as-electrodeposited films composed of the ZnO column-like crystals and the ZNR arrays. It can be seen from Fig. 7 that electrochemically fabricated ZNR arrays on the ITO glass substrate, though having air gaps between the ZNRs, exhibit high optical transmittance (about 90 %) in the visible range and a sharp absorption in the UV region, as shown in Fig. 7b. As compared to the ZNR arrays, the ZnO column film displays a low optical transparency in the visible range and a gradual absorption in the UV region. The possible light scattering dependent on the surface regularity could result in the difference in the optical transparency. The ZNRs are very highly oriented and vertically formed on the entire ITO substrate with nearly uniform diameter. Thus, the ZNR arrays have a low light scattering and a high optical transparency. Generally, the electrodeposited ZnO films or nanostructures exhibit band gap between 3.3 and 3.55 eV, depending on the structural morphologies and crystal defects. ZnO film, being a direct band gap semiconductor, has an absorption coefficient, which obeys the following relation photon energies: $(\alpha h\nu) = A(h\nu - E_g)^{1/2}$ [32], where A is a constant, α is the absorption coefficient (per centimeter) and $h\nu$ (electron volt) is the energy of excitation. The absorption coefficient α can be obtained by $\alpha = -\ln(T)/d$, where T is the transmittance and d is the thickness of film, respectively. In our case, both ZnO films used to estimate the band gap energy (E_g) almost have the same thickness. During the estimating on E_g, it was found the effect of the thickness on the estimate of E_g was negligible. Therefore, we assumed the absorption coefficient $\alpha \propto -\ln(T)$ in the fundamental absorption region, and better linearity was observed from the $(-\ln(T)\cdot h\nu)^2$ versus $h\nu$ plots (Inset in Fig. 7). The band gap of the ZNR arrays can be deduced by extrapolation of the plot of $(\alpha h\nu)^2$ versus $h\nu$ to the x-axis and found to be 3.37 eV or so, which is equal to that of the ZnO single crystal [33]. For the ZnO column film, its optical band gap red-shifts to 3.26 eV.

Raman scattering spectroscopy was performed to investigate the vibrational properties of the as-grown ZNR arrays in the range from 200 to 700 cm^{-1}. Several peaks are recognizable at 332.0, 378.7, 409.7, 437.3, and 582.2 cm^{-1} in the spectrum, as shown in Fig. 8. Since the crystalline structure of the ZnO films is a wurtzite type, which belongs to the space group C_{6v}^4, where all atoms occupy C_{3v} sites [34], the optical phonons at the Γ-point of the Brillouin zone belong to the following irreducible representation: $\Gamma = 1A_1 + 2B_1 + 1E_1 + 2E_2$, which are as follows:

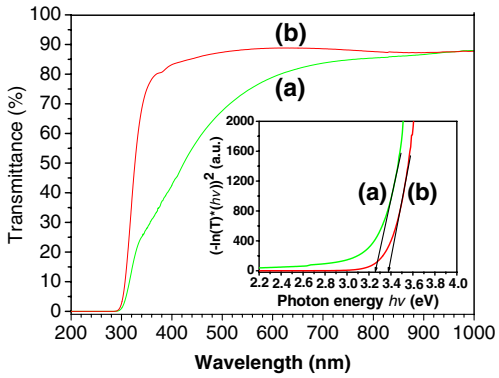

Fig. 7 Optical transmittance spectra of the as-electrodeposited films composed of the ZnO column-like crystals (**a**) and the ZNR arrays (**b**). The inset shows plot of $(-\ln(T)\cdot h\nu)^2$ versus photon energy of the as-electrodeposited films composed of the ZnO column-like particles (**a**) and the ZNR arrays (**b**)

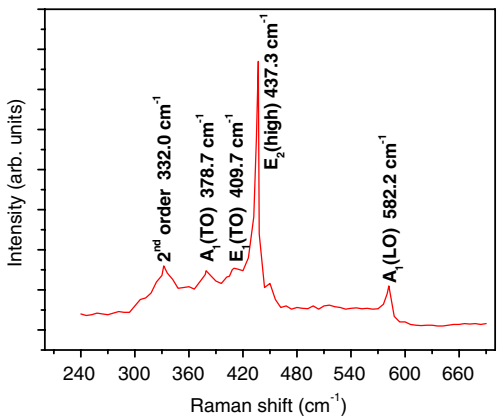

Fig. 8 Typical Raman scattering spectrum of the as-grown ZNR arrays on the ITO glass substrate from $Zn(NO_3)_2$ aqueous solution with HMT

E_2(low) at 101 cm^{-1}, A_1(transverse optical (TO)) at 380 cm^{-1}, E_1(TO) at 407 cm^{-1}, E_2(high) at 437 cm^{-1}, A_1(longitudinal optical (LO)) at 574 cm^{-1}, and E_1(LO) at 583 cm^{-1} [35]. Both the A_1 and E_1 modes are polar and capable of splitting into TO and LO phonons. E_2 mode is nonpolar but Raman-active. B_1 mode is neither polar nor Raman-active. The low frequency E_2 mode corresponds to the heavy Zn sublattices, while the high frequency E_2 mode is attributed to the oxygen sublattices. In light of these, the strongest peak centered at 437.3 cm^{-1} in Fig. 8 is assigned to the E_2(high) mode, which is characteristic of wurtzite-type phase of ZnO, and the weak peak at 582.2 cm^{-1} is in accordance with A_1(LO) mode. Two small peaks at 378.7 and 409.7 cm^{-1} corresponding to A_1(TO) and E_1(TO) modes are obvious. In addition, the peak at 332.0 cm^{-1} is believed to be attributed to the second-order Raman process from a multi phonon effect [35]. It is interesting to note that no peak was found for the E_1(LO) mode, which is directly related to low defects such as zinc interstitials and oxygen vacancies [36]. Generally, the appearance of the A_1(TO) and E_1(TO) modes can be attributed to the increasing contribution of scattering off the facets or sidewalls of the grains [37]. Therefore, the presence of sharp and strong peak of optical-phonon E_2(high) mode of ZnO with the absence of E_1(LO) mode and the weak A_1(TO) and E_1(TO) modes confirms that the synthesized ZNR arrays are highly crystalline with extremely low structural defects and well aligned in *c*-axis.

Photoluminescence measurements of the ZNR arrays were conducted at room temperature with an excitation wavelength of 325 nm. Figure 9 shows the typical RTPL spectrum in the wavelength range from 350 to 600 nm. A high intensity, sharp and strong peak centered at about 376 nm (3.37 eV) in the UV region was observed in the spectrum as well as a broad visible emission peak centered at 565 nm in the visible region. The UV emission also called as the near band edge emission originates from free

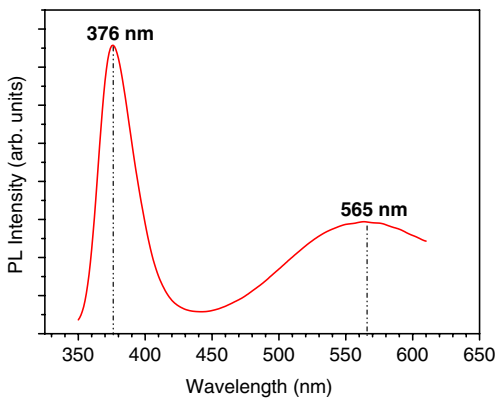

Fig. 9 RTPL spectrum of the ZNR arrays electrodeposited on the ITO glass substrate from $Zn(NO_3)_2$ aqueous solution with HMT

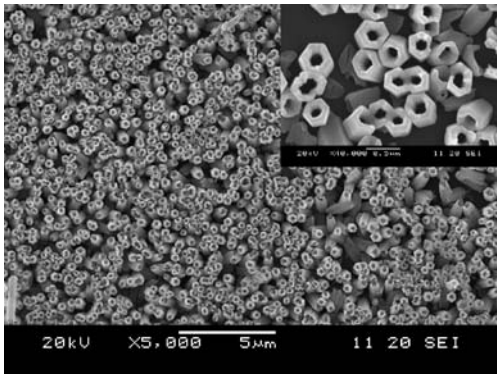

Fig. 10 Plan-view SEI of the ZNTs prepared based on the ZNRs by the second-step electrochemical dissolution process

excitonic emission in the ZnO materials [38]. The visible emission generally nominated as DLE is probably related to the variation of the intrinsic defects in ZnO films, such as zinc vacancy (V_{Zn}), oxygen vacancy (V_O), interstitial zinc (Zn_i), interstitial oxygen (O_i), and antisite oxygen (O_{Zn}). However, the exact intrinsic defect corresponding to each emission is still inconsistent and controversial. In view of above analysis, generally speaking, comparing the ratio of the relative PL intensity of the exciton emission to the DLE (I_{exc}/I_{DLE}) is a way to evaluate the quality of the ZnO films [6, 32]. Therefore, in our RTPL results, the high intensity ratio of I_{exc}/I_{DLE} in Fig. 9 is an evidence of the high quality of the ZNR arrays electrodeposited from the $Zn(NO_3)_2$ and HMT solution due to weak visible emissions from low intrinsic defects.

More importantly, the rapid synthesis of ZNRs could provide the feasibility for preparation of ZNTs within a shorter time by a subsequent electrochemical reaction. After the electrodeposition of ZNRs, the applied potential was reversed to 1.1 V versus SCE and the ITO substrate covered with ZNRs was used as a working electrode for the second-step electrochemical dissolution process in the fresh deionized water. Figure 10 shows the plan-view SEI of the ZNTs prepared based on the ZNRs. It can be seen that by the formation of hexagonal holes along the axes of the ZNRs, the ZNTs with wall thickness of several tens of nanometers and external diameter similar to that of the ZNRs were formed. Thus, the experimental result proves that the solid ZNRs can be selectively etched into hollow ZNTs by electrochemically generated acid from oxidation of water according to Eqs. 6 and 7. This selective etching mechanism is in accord with that reported earlier and attributed to the metastability of the (0001) plane and unbalanced distribution of defects on the (0001) plane [6]. Since the ZNTs were evolved from the ZNRs, the sizes of the ZNTs are directly determined by those of the electro-deposited ZNRs. All in all, the study on synthesis of the ZNRs by an HMT-assisted electrdeposition is of great

significance for the formation of the hierarchical ZnO structures as well as the ZNTs.

$$H_2O \rightarrow \frac{1}{2}O_2 + 2H^+ + 2e^- \quad (6)$$

$$ZnO + 2H^+ \rightarrow Zn^{2+} + H_2O \quad (7)$$

Conclusions

In summary, a soft and template-free electrochemical deposition method to prepare large-scale vertically aligned ZNR arrays on ITO glass substrates without ZnO seed layer from aqueous solution of 0.01 M $Zn(NO_3)_2$ containing HMT has been reported. The ZNR arrays grow along the *c*-axis direction perpendicular to the substrate. It has been shown that such ZNRs possess a high-quality single-crystal wurtzite structure. Optical characterization showed that the ZNR arrays exhibit high transmittance (90 %) in the visible wavelength range and the band gap energy blue-shifts to 3.37 eV, as compared with the generally electrodeposited ZnO films from the HMT-free aqueous zinc nitrate solution. Moreover, the presence of an optical-phonon E_2(high) at 437.3 cm^{-1} in Raman spectrum and strong and sharp ultraviolet emission at 376 nm but very weak defect-related deep level emission in the room temperature photoluminescence spectrum also indicated that such ZNR arrays are of good crystal quality. Moreover, the study on synthesis of the ZNRs by an HMT-assisted electrdeposition is of great significance for the formation of the hierarchical ZnO structures as well as the ZnO nanotube arrays.

Acknowledgments The authors thank Dr. Yaru Ni from Nanjing University of Technology for her assistance in photoluminescence measurements and Prof. Lisheng Huang from College of Sciences, Nanjing University of Technology for valuable discussions.

References

1. Li LS, Alivisatos AP (2003) Adv Mater 15:408
2. Yu HD, Zhang ZP, Han MY, Hao XT, Zhu FR (2005) J Am Chem Soc 127:2378
3. Pauzauskie PJ, Radenovic A, Trepagnier E, Shroff H, Yang PD, Liphardt J (2006) Nature Mater 5:97
4. Gao PX, Ding Y, Mai WJ, Hughes WL, Lao CS, Wang ZL (2005) Science 309:1700
5. Kim H, Kuk Y, Lee J, Kahng SJ, Son YW, Lee SB, Lee CK, Ihm J (2003) Phys Rev Lett 90:216107/1
6. She GW, Zhang XH, Shi WS, Fan X, Chang JC (2007) Electrochem Commun 9:2784
7. Masuda Y, Kinoshita N, Koumoto K (2007) Electrochim Acta 53:171
8. Tadashi S, Akira K (1974) Appl Phys Lett 25:10
9. Huang LS, Pu L, Shi Y, Zhang R, Gu BX, Du YW, Zheng YD (2005) Opt Express 13:5263
10. Sharma P, Sreenivas K (2003) Appl Phys Lett 83:3617
11. Hsueh TJ, Chen YW, Chang SJ, Wang SF, Hsu CL, Lin YR, Lin TS, Chen IC (2007) Sensor Actuat B-Chem 125:498
12. Park SH, Kim SH, Han SW (2007) Nanotechnology 18:055608
13. Basudev P, Batabyal KB, Amlan JP (2007) Sol Energy Mater Sol Cells 91:769
14. Wang X, Song J, Li P, Ryou JH, Dupuis RD, Summers CJ, Wang ZL (2005) J Am Chem Soc 127:7920
15. Choi JH, Tabata H, Kawai T (2001) J Crys Growth 226:493
16. Lee W, Jeong MC, Myoung JM (2004) Acta Mater 52:3949
17. Vayssieres L (2003) Adv Mater 15:464
18. Peulon S, Lincot D (1996) Adv Mater 8:166
19. Tena-Zaera R, Elias J, Wang G, Lévy-Clément C (2007) J Phys Chem C 111:16706
20. Otani S, Katayama J, Umemoto H, Matsuoka M (2006) J Electrochem Soc 153:C551
21. Chen QP, Xue MZ, Sheng QR, Liu YG, Ma ZF (2006) Electrochem Solid-State Lett 9:C58
22. Chander R, Raychaudhuri AK (2008) Solid State Commun 145:81
23. Cui JB, Soo YC, Chen TP (2008) J Phys Chem C 112:4475
24. Gao YF, Nagai M, Masuda Y, Sato Y, Koumoto K (2006) J Cryst Growth 286:445
25. Wellings JS, Chaure NB, Heayens SN, Dharmadasa IM (2008) Thin Solid Films 516:3893
26. Mahalingam T, John VS, Raja M, Su YK, Sebasyian PJ (2005) Sol Energy Mater Sol Cells 88:227
27. Fahoume M, Maghfoul O, Aggour M, Hartiti B, Chraïbi F, Ennaoui A (2006) Sol Energy Mater Sol Cells 90:1437
28. Goux A, Pauporté T, Chivot J, Lincot D (2005) Electrochim Acta 50:2239
29. Gao XD, Li XM, Yu WD (2005) J Phys Chem B 109:1155
30. Vayssieres L (2004) Int J Nanotechnol 1:1
31. Yoshida T, Komatsu D, Shimokawa N, Minoura H (2004) Thin Solid Films 451-452:166
32. Gu CD, Li J, Lian JS, Zheng GQ (2007) Appl Surf Sci 253:7011
33. Peulon S, Lincot D (1998) J Electrochem Soc 145:864
34. Umar A, Hahn YB (2006) Nanotechnology 17:2174
35. Xu CX, Sun XW, Zhang XH, Ke L, Chua SJ (2004) Nanotechnology 15:856
36. Chen Y, Bagnall DM, Koh HJ, Park KT, Hiraga K, Zhu Z, Yao T (1998) J Appl Phys 84:3912
37. Wang YD, Chua SJ, Tripathy S, Sander MS, Chen P, Fonstad CG (2005) Appl Phys Lett 86:071907
38. Greene LE, Law M, Goldberger J, Kim F, Johnson JC, Zhang YF, Saykally RJ, Yang PD (2003) Angew Chem Int Ed 42:3031